SOFT ROBOTS

Grasping with kirigami shells

Yi Yang, Katherine Vella, Douglas P. Holmes*

Copyright © 2021 The Authors, some rights reserved; exclusive licensee American Association for the Advancement of Science. No claim to original U.S. Government Works

The ability to grab, hold, and manipulate objects is a vital and fundamental operation in biological and engineering systems. Here, we present a soft gripper using a simple material system that enables precise and rapid grasping, and can be miniaturized, modularized, and remotely actuated. This soft gripper is based on kirigami shells—thin, elastic shells patterned with an array of cuts. The kirigami cut pattern is determined by evaluating the shell's mechanics and geometry, using a combination of experiments, finite element simulations, and theoretical modeling, which enables the gripper design to be both scalable and material independent. We demonstrate that the kirigami shell gripper can be readily integrated with an existing robotic platform or remotely actuated using a magnetic field. The kirigami cut pattern results in a simple unit cell that can be connected together in series, and again in parallel, to create kirigami gripper arrays capable of simultaneously grasping multiple delicate and slippery objects. These soft and lightweight grippers will have applications in robotics, haptics, and biomedical device design.

INTRODUCTION

Grasping and manipulating objects is an essential part of daily life for both humans and robots. Humans can perform precise grasping and manipulation based on their hand morphology (*1*), and hand morphology has inspired a variety of robotic gripper designs ranging from linkage-based hard grippers to soft grippers. Although the mechanics and kinematics of robotic grasping have been extensively investigated (*2*), grasping in unstructured environments and handling slippery, deformable, and fragile objects, even when assisted by either adaptive end effectors or computer vision and learning, are still grand challenges in the frontier of robotic grasping and manipulation (*3*).

Compliant end effectors are an emerging technology for human-machine interactions and are highly desired in biomedical applications (*4*), food packaging (*5*), and rehabilitation (*6*). Compliance, or softness, enables the gripper to grasp unfamiliar objects and objects that are in unstructured environments. Innovations in soft gripper design include novel design forms, such as tentacle or finger-based grippers (*7*, *8*, *9*, *10*), anthropomorphic soft hands with fingers and palm (*11*, *12*), and a universal gripper (*13*). Depending on their deformed configuration, these grippers may perform power grasping by enveloping an object with multiple contact points, precision grasping by pinching an object with one contact point per finger, or both (*14*, *15*, *16*). Enveloping objects through gentle power grasping has been realized using the pneumatic and hydraulic actuation of soft, architected elastomers (*17*, *18*, *19*, *13*). Reliance on fluid actuation is limiting, because it requires external tethered support, it can be difficult to adapt to different environments, and the physical limits of soft lithography restrict miniaturization (*20*). The requirement of an additional, tethered support system and challenges with miniaturization also occur in cable-driven actuation (*21*). Alternatively, soft grippers may be actuated by the deformation of stimuli-responsive materials (*22*), which can deform in response to light (*23*), temperature (*24*), electric (*25*), magnetic (*26*), and chemical (*27*) stimuli. These materials may pave the way to multiscale, untethered grasping; however, stimuli-responsive materials often sacrifice response speed and precision.

Softness, broadly defined, is a function of both material and geometry. The extremely high compliance of slender structures—regardless of their modulus of elasticity—enables them to bend and conform to various shapes (*28*), making them an ideal candidate for grasping (*29*, *30*). Compliant mechanisms enable various design strategies to provide shape morphing and grasping motions by obtaining kinematic motion from the finite deformation of structural components (*29*, *31*). Through the bending of flexible members or rigid elements connected with flexible hinges, complex motion can be achieved from simple topological designs (*32*), such as origami-inspired shape morphing mechanisms (*33*, *34*, *35*). In general, although the force transmission of soft grippers is limited compared with rigid robotic grippers, their compliance increases the grippers' adaptability, allowing autonomous grasping and manipulation on objects with irregular shapes, especially in compact spaces and unstructured environments (*36*, *29*). Recently, by taking inspiration from the paper-cutting arts of kirigami, engineers have been able to spatially tailor the stiffness of thin sheets by using cuts. Distinct from the shape-shifting of an origami sheet, which is mainly governed by folding pattern geometries, shape-shifting of a kirigami sheet is governed by pattern geometry, topology, and external loads that induce stretching, bending, and twisting (*37*, *38*, *39*, *40*, *41*). Despite the various possible kirigami tessellations, linear parallel cuts (*42*) are often used to create architected materials (*43*, *44*, *37*, *45*, *46*) and mechanical and electrical devices (*42*, *47*, *48*, *49*, *50*) across multiple length scales due to their simplicity and mathematically predictable behaviors. The geometry of this pattern is characterized by the length (ℓ_c) and width (t_c) of a single slit and the longitudinal (ℓ_y) and transverse spacing (ℓ_x) between adjacent slits (Fig. 1 and Movie 1). By controlling these geometric parameters in the tessellation, deformed configurations upon uniaxial stretching can be programmed a priori (*46*).

In this work, we present a simple design strategy for soft grippers enabled by the predictable deformation of kirigami shells that are capable of rapid and precise grasping of delicate objects and can be miniaturized, serialized, and untethered. Using experiments, finite element simulations, and theoretical modeling, we show that this gripper is scalable and material independent and can be actuated by

Department of Mechanical Engineering, Boston University, 110 Cummington Mall, Boston, MA 02215, USA
*Corresponding author. Email: dpholmes@bu.edu

Downloaded from https://www.science.org at The Hong Kong University of Science and Technology (Guangzhou) on May 26, 2026

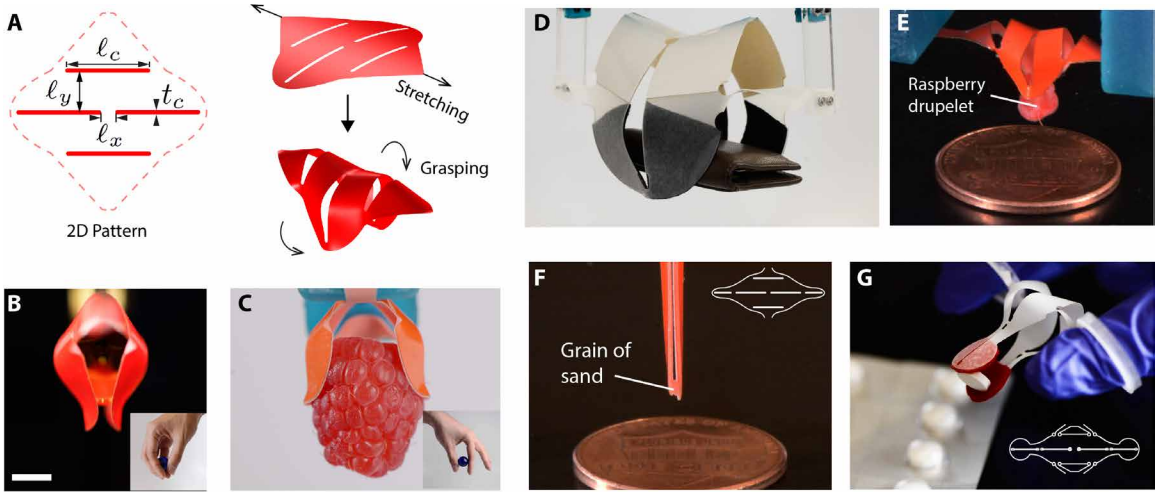

Fig. 1. Demonstration of a kirigami shell as a soft gripper. (**A**) 2D geometry of kirigami shell and its morphology upon stretching. Performing thumb-index finger gripping: holding/caging a hydrogel sphere (**B**) and pinching a raspberry (**C**). Scalable grippers: a hand-size gripper pinching a wallet (**D**) and a coin size gripper pinching a raspberry drupelet (**E**). (**F**) Gripper with extended appendages gripping a grain of sand. (**G**) Portable hand tool gripping medical pill using modified appendages. Scale bar, 10 mm.

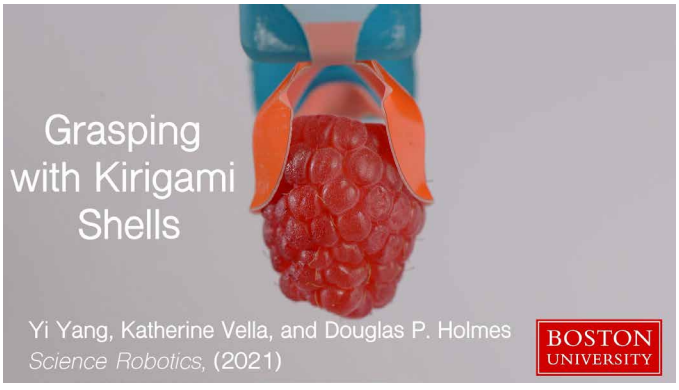

Movie 1. Grasping with kirigami shells. The versatility of kirigami grippers allows them to collect a wide range of objects, including something as delicate as a raspberry. They can be scaled up to grasp large objects and down to grasp an individual grain of sand. Connecting kirigami gripper unit cells in series and/or in parallel enables them to grasp slender objects and manipulate multiple objects simultaneously. These structures can be made of a variety of materials, and we demonstrate how to actuate the grippers using a magnetic field.

simply stretching the kirigami shell. We find that a shell with a four-petal flower shape, composed of four arranged slits, is the most fundamental form of kirigami shell that can transfer a linear uniaxial actuation to a more complicated grasping motion (Fig. 1A). When the kirigami shell is fully closed, it forms a capsule, giving rise to two grasping postures, pinching with appendages or enveloping with the capsule. Enveloping, which provides many contact points between gripper and objects, is a very effective grasping scheme to secure objects, especially for capturing slippery and delicate objects.

We have integrated the kirigami gripper onto a commercially available robotic arm to rapidly and precisely grasp a variety of objects with different shapes and stiffness (Fig. 1, B and C, and movie S1). Figure 1 (B and C) shows that the kirigami shell grasps a hydrogel sphere and a raspberry, respectively, mimicking human hand–gripping postures (*1*). Because of the simplicity of fabrication and actuation, which we detail below, the size of the shell can be scaled (Fig. 1, D and E), and the shape of the appendages can be customized (Fig. 1, F and G) to grasp millimeter-scale objects, such as a raspberry drupelet (Fig. 1D), or microscale objects, such as a single grain of sand (Fig. 1F). We also demonstrate how the kirigami shell can be made into a tool that can be used by a hand, or picked up by a robotic end effector, to perform gentle and precision grasping by gripping a medical pill (Fig. 1G). Such a hand tool would be portable and easy to actuate and thus may have potential to assist people with hand deformities and disorders. Moreover, we demonstrate a kirigami gripper array relocating multiple objects into spatially organized layout similar to transfer printing (*51*, *52*) and an untethered kirigami gripper that is remotely actuated by a magnetic field to capture a falling object in 60 ms.

RESULTS

Shape morphing of kirigami shells

To fabricate kirigami shells, we used a polyethylene terephthalate (PET) sheet with an average thickness of 0.127 mm. A particular kirigami two-dimensional (2D) precursor was then patterned onto the PET sheet via laser cutting. Then, the kirigami sheet was mounted onto a stainless steel cylinder with a radius of r_0 and heated in oven for 1 hour to form a kirigami cylindrical shell with a single principal curvature of $\kappa_0 = 1/r_0$ (Fig. 2A). This cylindrical curvature with a finite, arbitrary magnitude would trigger the shell to warp into a cylindrical metasurface upon stretching. We find that this deformation does not depend notably on the size or overall geometry of the kirigami shell but is governed by the geometric parameters shown in Fig. 1A (note S1). The curved edge used here is a half-circle with a radius of ℓ_y. To understand the morphology and provide a road map for theoretical modeling, we used experiments and numerical simulations [finite element analysis (FEA)] to perform uniaxial tensile tests on kirigami shells. The mechanical response as we quasi-statically stretch the end by controlling the displacement is shown in Fig. 2B (movie S2). Similar to a typical stress-strain curve for soft elastic materials, we observed a nearly linear deformation in the

Downloaded from https://www.science.org at The Hong Kong University of Science and Technology (Guangzhou) on May 26, 2026

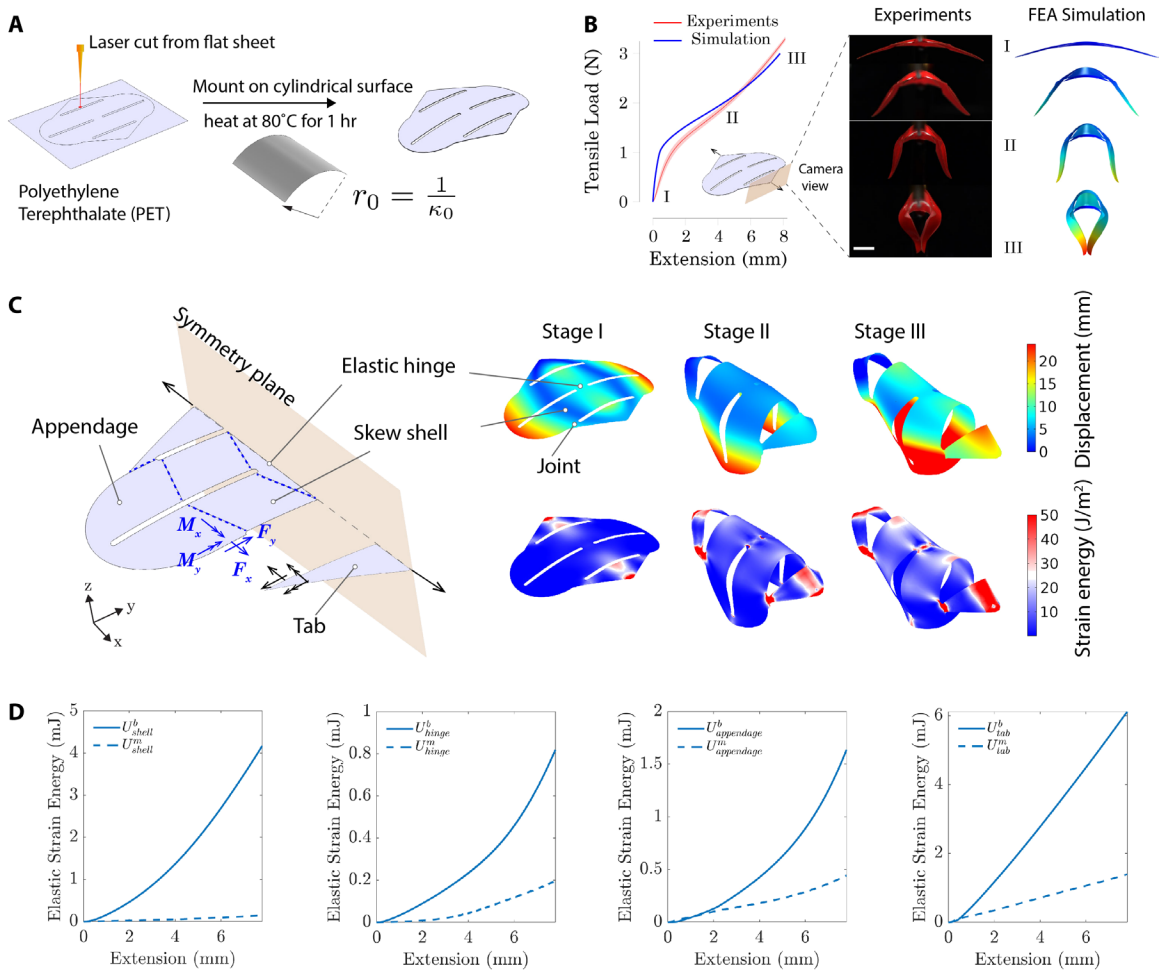

Fig. 2. Shape morphing of kirigami shell. (**A**) Fabrication of kirigami patterned thin shell. (**B**) Experiment and FEA simulation showing a typical mechanical response of kirigami shell under uniaxial tension. The solid line represents the averaged results, and the shaded area represents the standard deviation. (**C**) Free-body diagram illustrating the structural decomposition for mechanical modeling and FEA results showing displacement and strain energy during shape morphing. (**D**) FEA results showing variation of elastic membrane energy (U^m) and bending energy (U^b) in the decomposed structural components in terms of the applied extension. Scale bar, 10 mm.

initial stage (stage I) followed by a stiffness softening (stage II). Instead of stopping the extension at failure due to the propagation of the cuts, or crack tips, we stopped the extension when the kirigami shell is just fully closed (stage III). The maximum von Mises stress occurs at the tips of the slit due to stress concentration (note S2), which can be further reduced by increasing the radius of the rounded slit tips.

On the basis of our observations of the deformation of the kirigami shell from initial stretching to final closure, we decompose the kirigami shell into four kinds of structural components: (i) two handling tabs, (ii) four shells (parallelogram shells), (iii) a central elastic hinge, and (iv) two appendages (Fig. 2C). Because the thickness of shell is much smaller than any other dimension, we ignore the variation of stresses through the thickness. A free-body diagram of static analysis shows the internal forces (F_x, F_y) acting on the cross-section of the joint connecting tab and the edge of the skew shell (Fig. 2C). The function of the handling tab is primarily transferring the uniaxial tensile load to the shells through the internal forces and moments. The configuration of the tab may not alter its functionality (note S2). Because of the existence of natural curvature (κ_0), additional internal bending moments (M_x, M_y) will be introduced. Because the shear effect through the thickness is ignored for thin shells, deformation caused by the forces and moments would only generate internal stretching and bending strains (*53*). To visualize the contribution from bending and stretching, we first plot the elastic strain energy per unit area on the surface of the kirigami shell at the three deformation stages (Fig. 2C). Next, we plot the bending energy and membrane energy from each structural component as a function of the extension (Fig. 2D). We observe that bending energy dominates the elastic strain energy in all structural components, which contributes 96.4%, 81.7%, 73.5%, and 80.1% of the elastic strain energy in shells, hinge, appendages, and tabs, respectively. This percentage is lower in components that contain tips of the slits and loading points where local stretching causes higher membrane energy. We also notice that the strain energy in the appendage is significantly lower than that in the shells and the hinge, except near the slit tip. Therefore, we consider the shells and central elastic hinge to be the active shape-shifting components, whereas the appendages

Downloaded from https://www.science.org at The Hong Kong University of Science and Technology (Guangzhou) on May 26, 2026

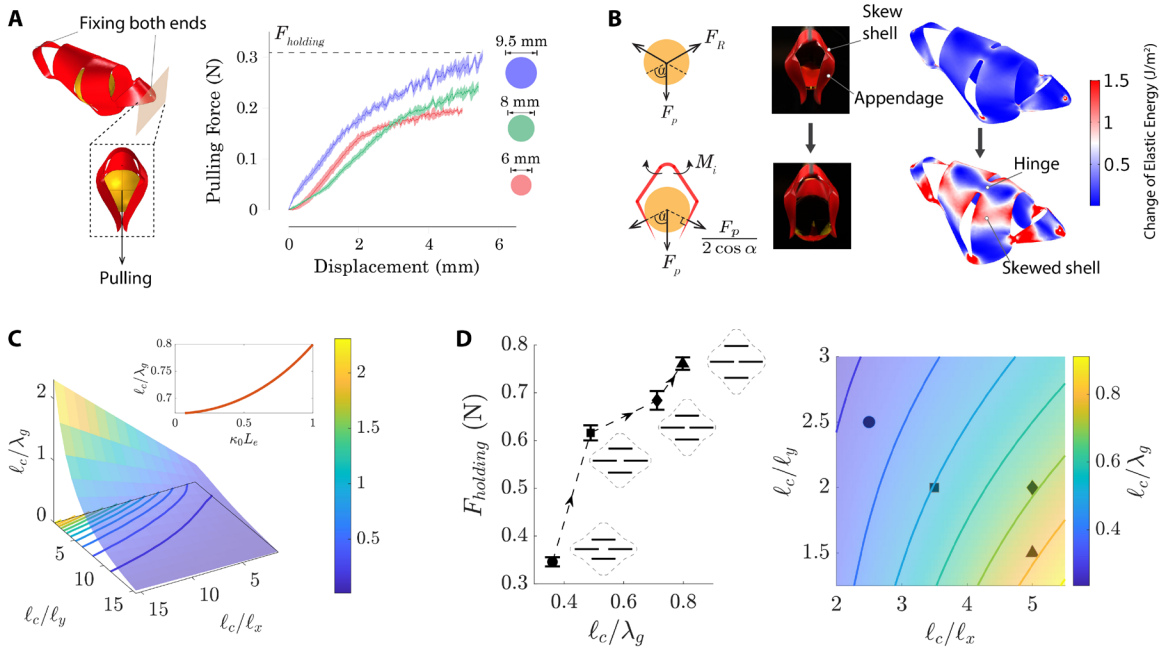

Fig. 3. Rational design for gripping performance. (**A**) Pulling-out tests of object size effect on holding force, schematics, and experimental results. (**B**) Schematics for static analysis and FEA simulations illustrating change of elastic energy during pulling test. (**C**) Nondimensionalized gripper characteristic length (ℓ_c/λ_g) as a function of the 2D geometric parameters (ℓ_c/ℓ_x, ℓ_c/ℓ_y) and natural curvature for shell with a constant thickness. (**D**) Experimental results showing that holding force increases monotonically as navigating through the nondimensionalized gripper characteristic length landscape.

are underactuated and can be varied (note S3), and the tabs are primarily used for handling.

Rational design for gripping performance

Because we demonstrated the morphology and the grasping functionality of the kirigami shell gripper, we next use experiments and modeling to quantitatively evaluate the robustness to external forces. Robustness of a gripper to external forces is defined as the maximum pull-out force the gripper can resist (*7*, *54*). It is also the enveloping holding force, typically measured by the force required to pull a target object out of the gripper (*13*). In general, this holding force depends not only on the weight but also on the geometry and the size of the object. For the sake of simplicity and to capture the essential gripping mechanism, we select spheres with various radii (R) as the target objects. On the basis of this metric, we performed pull-out tests in which a sphere was first enveloped in a fully closed kirigami shell gripper and then was quasi-statically pulled out (Fig. 3A).

To understand the effect of object size on identifying the relationship between the kirigami pattern geometry and the gripper's robustness, we investigate the holding force with constant kirigami geometric parameters of $\ell_c/\ell_x = 5$ and $\ell_c/\ell_x = 2$ using three 3D-printed spheres (R=3, 4, and 4.75 mm). Figure 3A shows that the holding force ($F_{holding}$) increases monotonically with the increase of the sphere's radius. When the gripper is fully closed, the contact angle (α) is identical to all three spheres. As the sphere is pulled, α increases until reaching about $\pi/2$, where the pulling force (F_p) approaches its maximum value ($F_{holding}$) and the sphere is pulled out (Fig. 3B). At this point, the distance separating the appendages approximately equals to the diameter of the sphere ($2R$). A simple static analysis without friction (note S4) shows that this reaction force, denoted by F_R, is balanced with the pulling force and can be calculated by $F_R = F_p/(2\cos\alpha)$. Therefore, pulling a sphere with a larger diameter leads to larger deformations of the shells, which produce a higher resisting force from the appendages to the sphere.

Seeking a theoretical explanation of how kirigami pattern geometry relates to robustness, we derived a simplified closed-form theoretical model using energy methods. On the basis of the conservation of mechanical energy, the work done by F_p must be equal to the change of elastic energy in the gripper to pull out the sphere. A conservative assumption is to ignore the interfacial friction (note S4) and local deformation between sphere and appendages for evaluating the robustness. Because the elastic energy is dominated by bending, we can approximate the total elastic energy of the active shape-shifting components, i.e., the skew shells and hinge, with the total bending energy $U^b = U_s^b + U_h^b$, where U_s^b and U_h^b denote bending energy of the skew shell and hinge, respectively. From the FE simulation, we observed that the change of elastic energy mainly occurs in the shells as the sphere was pulled, except in regions where stress was concentrated (Fig. 3B and movie S3). During the closure process, elastic energy stored in the shape-shifting components is $U_s^b + U_h^b$. During the pull-out process, elastic energy converted to the external work done is mainly U_s^b. Thus, to pull out the sphere, we assume that work done by F_p only needs to overcome a certain amount of U_s^b without changing U_h^b. In other words, the robustness is correlated to the ratio of $U_s^b/(U_s^b + U_h^b)$.

Using shell theory, we model the shape-shifting of the skew shell and the hinge as bending of a cylindrical thin shell along its transverse direction and its axis direction, respectively. By assuming a linear elastic material response, the bending energy of the skew shell is given by (note S5)

Downloaded from https://www.science.org at The Hong Kong University of Science and Technology (Guangzhou) on May 26, 2026

$$U_s^b = \frac{D(\ell_y - t_c)\varphi_0^3}{L_e^3[\varphi_0 + 2\varphi_0\sin^2\varphi_0 + \sin\varphi_0(3\cos\varphi_0 - 4)]}\delta^2 \quad (1)$$

and the bending energy of the hinge is given by

$$U_h^b = \frac{4(1+\nu)D\ell_x\varphi_0^2\sin\varphi_0}{L_e^2[\varphi_0 + 2\varphi_0\sin^2\varphi_0 + \sin\varphi_0(3\cos\varphi_0 - 4)]}(\theta \cdot \delta) \quad (2)$$

where $D = \frac{Eh^3}{12(1-\nu^2)}$ is the shell's bending rigidity defined by Young's modulus E, shell thickness h, and Poisson's ratio ν. The effective length $L_e = \sqrt{\left(\frac{\ell_c}{2} - \frac{\ell_x}{2}\right)^2 + (\ell_y - t_c)^2}$ is used to relate a parallelogram-shaped cylindrical shell to a rectangular shell (*46*). The nondimensional natural curvature of the cylindrical shell is given by $\varphi_0 = \kappa_0 L_e$. Last, δ is the vertical displacement and θ is the angle of rotation of the skew shell and the hinge (note S5). Then, the energy ratio is expressed as

$$\frac{U_s^b}{U_s^b + U_h^b} = \frac{1}{1 + \lambda_g\theta/\delta} \quad (3)$$

Here, we define a gripper characteristic length λ_g as

$$\lambda_g = 4(1+\nu)\frac{\ell_x\sin(\kappa_0 L_e)}{(\ell_y - t_c)\kappa_0} \quad (4)$$

Through mathematical manipulation, we nondimensionalize this equation by the slit length ℓ_c and express ℓ_c/λ_g in terms of ℓ_c/ℓ_y and ℓ_c/ℓ_y as

$$\frac{\ell_c}{\lambda_g} = \frac{\ell_c\kappa_0\left(\frac{\ell_y}{\ell_c} - \frac{t_c}{\ell_c}\right)}{4(1+\nu)\frac{\ell_x}{\ell_c}\sin(\kappa_0\ell_c\sqrt{\left(\frac{1}{2} - \frac{\ell_x}{2\ell_c}\right)^2 + \left(\frac{\ell_y}{\ell_c} - \frac{t_c}{\ell_c}\right)^2})} \quad (5)$$

We find that ℓ_c/λ_g decreases monotonically as both ℓ_c/ℓ_x and ℓ_c/ℓ_y increase for a given curvature, $\kappa_0 = 0.35\ \mathrm{mm}^{-1}$ (Fig. 3C). In addition, ℓ_c/λ_g also increases monotonically as φ_0 increases for given geometric parameters ($\ell_c/\ell_x = 5$, $\ell_c/\ell_y = 2$). Because $U_s^b/(U_s^b + U_h^b)$ is a monotonic function of ℓ_c/λ_g, we expect that the robustness to external forces is also a monotonic function of ℓ_c/λ_g, i.e.

$$F_{\mathrm{holding}} \sim \frac{\ell_c}{\lambda_g} \quad (6)$$

Because t_c is small compared with ℓ_c and ℓ_y in our kirigami patterns ($\ell_c/t_c \approx 20$, $\ell_y/t_c \approx 10$), we neglect the impact of the slit width in the subsequent analysis. To validate the theoretical model, we performed pulling tests with a 3D-printed sphere (R= 4 mm) and four kirigami shells of varied geometry characterized by (ℓ_c/ℓ_x, ℓ_c/ℓ_y) of (2.5, 2.5), (3.5, 2.0), (5.0, 2.0), and (5.0, 1.5), with t_c= 0.8 mm for each (Fig. 3D). As predicted by the model, when we navigate the geometric landscape from downhill side, marked by a circle, to uphill side, marked by a triangle, the holding force increases monotonically as the increasing of ℓ_c/λ_g. The corresponding 2D precursor of each gripper is also shown in Fig. 3D near its marker.

The appendages are underactuated components, and that means that the passive deformation of the thin shell buffers the force transmission between actuation and pinching. A lower force transmission enables the gripper to delicately grip objects of variable stiffness without adjusting the applied actuation. The pinching force acting from the appendages to the sphere is the horizontal component of the reaction force, $F_R\sin\alpha$. Thus, the force transmission also monotonically grows with ℓ_c/λ_g (fig. S6). To demonstrate the actuation buffer capacity, we attached the kirigami shell to a commercially available two-finger robotic gripper (Robotiq model Hand-E) driven by an industrial robotic arm (Universal Robots model UR5) to grip various objects ranging from rigid objects like a stone to soft and fragile objects like a raspberry. For a classic two-finger gripper, to perform such a task without damaging the target object, the traveling distance of the fingers needs to be adjusted based on the size and stiffness of the target. By simply attaching the kirigami shell to the robotic gripper, there is no need to adjust the traveling distance due to the fact that kirigami shell adapts itself to the actuation by storing elastic energy in the shell without feedback control.

Modular gripper array

Transfer printing techniques perform precise and deterministic manipulation of materials in micro-/nanoscale device fabrication (*52*). In robotic manipulation on the other hand, such delicate and precise manipulation of multiple objects simultaneously has not been practically realized. The ability to simultaneously grasp many objects is of particular importance for efficient food handling and packaging using robotics (*5*). To show the potential impact of these grasping mechanics, we demonstrate a unique capability designed for collecting and relocating multiple spatially organized objects without changing their relative orientation in one grasping operation using a modular gripper array.

The modular kirigami shell gripper can be assembled into several configurations by patterning the unit cell in series, in parallel, or both to exhibit different griping capabilities. By simply repeating the unit cell in series, a gripper array can be achieved as illustrated in Fig. 4A, where the unit cell is highlighted in blue. To grasp multiple objects, we identified the grasping acquisition region (*7*, *55*) and grasping repeatability of a single shell gripper with small sphere (note S6). For a grasping operation repeated 100 times, the success rate is defined as the percentage of successful grasping operations, where a grasping operation consisted of picking up an object and placing it in the assigned container, and ranges from 70 to 100% (fig. S7A). Here, the success rate of grasping small objects measures the repeatability and precision of the robotic grasping operation. For shallow shells, the acquisition region is about the same as the shell area projected on the grasping surface. Figure 4B illustrates that within the acquisition region, individual hydrogel spheres with different sizes were automatically collected and moved into individual unit cell grippers by the appendages of the gripper array when stretched at the holding tabs.

In addition, each N-by-1 array can also be placed in parallel. By replacing the fingers of the Robotiq Hand-E with a custom-built connector, we can directly integrate the gripper array to the Universal Robots UR5 robotic arm. Figure 4C demonstrates the open and closed configuration of an 8-by-3 gripper array. Because the gripper is fabricated with a thin shell of PET, we attached an additional felt layer (red) on the appendages to cover the sharp edge and prevent potential damage to the target objects. We precisely picked up and relocated 24 hydrogel spheres, from an 8-by-3 matrix configuration to an 8-by-3 matrix configuration, in one grasping operation (Fig. 4D and movie S4). Each hydrogel sphere was gripped delicately and placed precisely in the desired location.

Downloaded from https://www.science.org at The Hong Kong University of Science and Technology (Guangzhou) on May 26, 2026

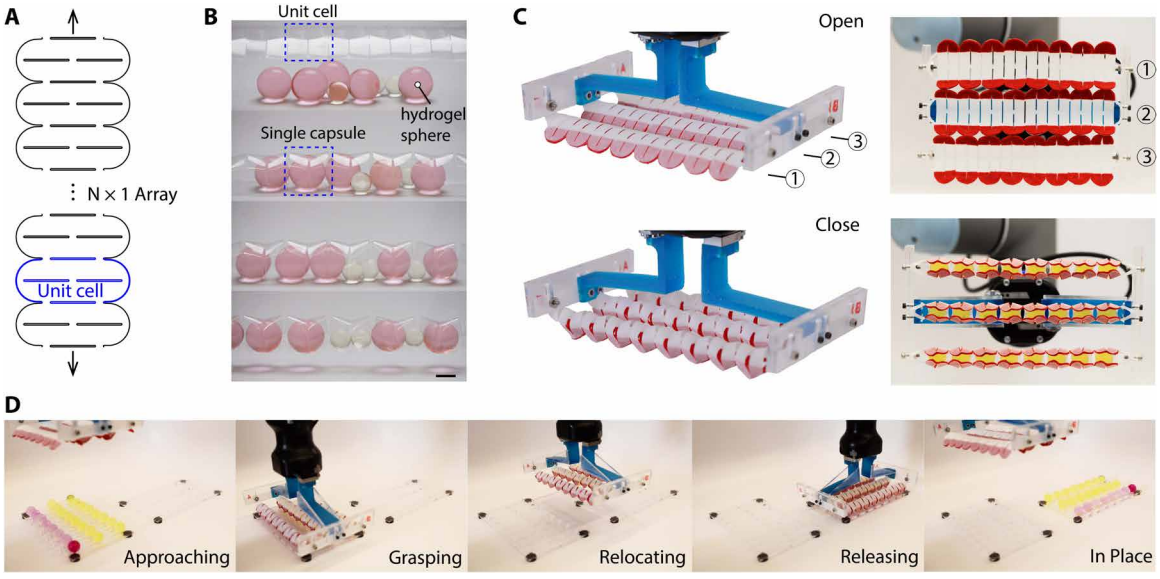

Fig. 4. Demonstration of kirigami shell gripper array. (**A**) Schematic drawing of a kirigami gripper array composed of *N* unit patterns in series. (**B**) Automatic aligning of multiple objects into each unit capsule of an *N*-by-1 gripper array within the acquisition region. The gripper is fabricated from transparent PET to show the inner view. (**C**) Photo images showing an 8-by-3 gripper array prototype. A felt layer (red) was added to the appendages to avoid sharp edges for grasping hydrogel spheres (yellow). (**D**) Precision grasping and placing of 24 hydrogel spheres in one grasping operation. Scale bar, 10 mm.

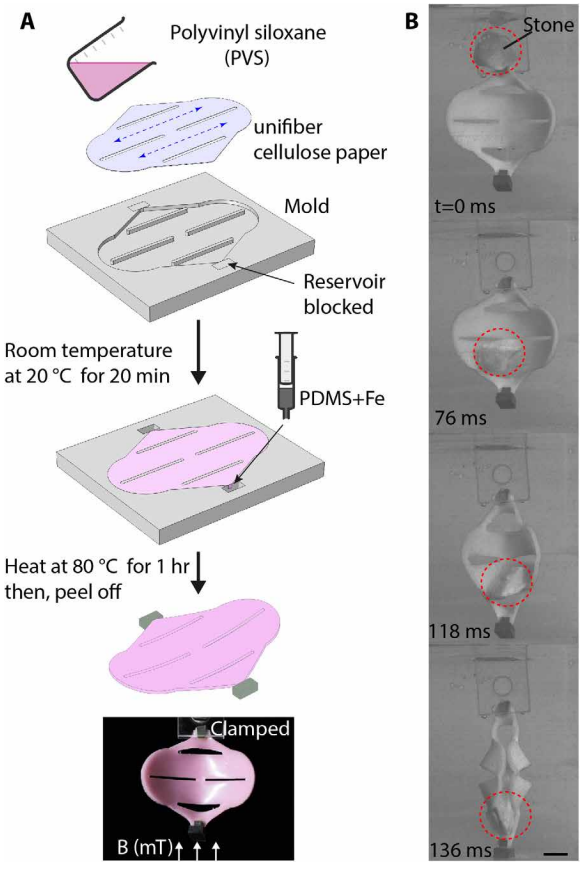

Fig. 5. Demonstration of rapid grasping under magnetic actuation. (**A**) Fabrication of magneto-kirigami gripper. (**B**) High-speed camera images showing capture of a free-falling stone in an aquatic environment in a magnetic field with a constant magnetic flux. Scale bar, 10 mm.

Untethered magnetic actuation

Because grasping via a kirigami shell is a mechanics-based approach that is independent of the constituent materials and applied actuation stimulus, here, we demonstrate a rapid untethered actuation using a remote magnetic field. External magnetic actuation is recognized as a long-range untethered actuation with high response speed and precision, which are highly desired in surgical robots and drug delivery (*56*, *57*). Instead of generating structural compliance from a thin sheet of a hard material, such as PET (Young's modulus ≈ 3.5 GPa), the kirigami shell is fabricated with an elastomer [polyvinylsiloxane (PVS)]–based soft composite material.

As shown in Fig. 5A, we poured uncured PVS into a patterned mold filled with cellulose paper. This cellulose paper has uniaxially aligned fibers, which are schematically shown as blue dashed lines in Fig. 5A. We introduced this anisotropic material with the PVS for two reasons: (i) it produces a differential absorption through the thickness, giving rise to the formation of a cylindrical curvature perpendicular to the fiber direction and (ii) it enhances the strength and stiffness of the PVS polymeric matrix (the Young's elastic modulus of this composite is about 8 MPa). After the PVS cured, two end blocks covering the reservoirs were removed. Then, these reservoirs were injected with iron particles (≈3 μm in diameter) mixed in uncured polydimethylsiloxane (PDMS) (weight % ≈ 3:1) and placed in the oven for 1 hour at 80°C. The PVS and PDMS elastomers are chemically very similar, so there is a strong adhesion at the interface between these two materials. The silicone rubber kirigami grippers had a thickness of $h = 1.1$ mm and $\varphi_0 = 0.31$.

Despite the weak ability to retain remnant magnetization upon removal of external magnetic field, the Fe-PDMS composite block responds to the magnetic field rapidly and provides enough actuation force to close the gripper. Quasi-static tests were performed to obtain the force required for closure (fig. S9A), and dynamic tests were performed to identify the response speed under magnetic actuation (fig. S9B). As shown in Fig. 5B, the gripper is fully submerged

Downloaded from https://www.science.org at The Hong Kong University of Science and Technology (Guangzhou) on May 26, 2026

in water vertically, clamped at the top, and surrounded by a magnetic field with a constant magnetic flux of $B \approx 27.6$ mT. At this magnetic flux density, the force balance between magnetic force and elastic restoring force of the ferromagnetic end (bottom) is in static equilibrium. A free-falling limestone was released from the water surface, whose motion was captured using a high-speed digital camera (Photron FASTCAM Mini; movie S5). When the falling stone touches the gripper, it perturbs the static balance, leading to the closure of the gripper actuated by the magnetic field. Because the response speed of the kirigami gripper ($t \sim 60$ ms) is less than the time required to travel across the gripper, the limestone is captured by the gripper.

DISCUSSION

In summary, we have developed a soft gripper design that has a simple form and robust dexterity. The kirigami gripper enables an integrated solution combining scalability and remote control without sacrificing operation speed and precision. With magnetic actuation, the soft gripper can grasp an object in milliseconds. In addition, it can be modularized to perform more complicated grasping operations, such as gripping and aligning multiple objects in one grasping operation. This remains a challenge for many existing robotic grippers. In addition, we also developed a portable hand tool using the kirigami gripper, which may serve as a haptic assistant tool for people with hand deformities and disorders. We envision that the kirigami gripper will lead to a broad range of applications in robotics, human-machine interactions, and health care.

The kirigami gripper combines advantages of both hard and soft grippers to create a simple, low-cost, rapid, precise, and remotely controllable soft gripper. There are open questions that remain to be addressed to use these structures. Although the gripper is mechanics-based and material-independent, materials used to build the gripper need to sustain moderate elastic strains, e.g., elastomers. Elastoplastic materials, such as PET, can also be used if moderate plastic deformation could be tolerated at the tip of the slit. In addition, because bending energy is a cubic function of the thickness, $U_s^b \sim h^3$, as we scale up the size of the gripper, in meters for example, input energy required to close the gripper increases significantly. Our model suggests that reducing the thickness of the hinge relative to the skew shells when scaling up the gripper may help reduce the force required to actuate without reducing the robustness. However, such an increase in energy cost is not an issue as we scale down the gripper in meso-, micro-, or nanoscale. Kirigami design and fabrication has been implemented extensively in micro- and nanoscale (*43*, *44*, *45*); we expect that the application of this proposed grasping mechanism may have an impact in microrobots with microscale fabrication techniques.

Moreover, the ferromagnetic material used here for remote magnetic actuation is pure iron microparticles, which easily lose the induced magnetization upon removal of external magnetic field. By incorporating hard magnetic materials that have high coercivity, such as neodymium-iron-boron (NdFeB), more complex motion may be achieved. For example, if the ferromagnetic blocks at the tip of the handling tab (Fig. 5A) are magnetized, a magnetic-guided locomotion or cargo delivery may be possible. Besides magnetic actuation, we anticipate that the kirigami shell could also be actuated through other external stimuli when incorporated with corresponding stimuli-responsive materials.

MATERIALS AND METHODS

PET films

The PET film was produced by Dupont Teijin Films. Two types of the PET films were used in the experiment: transparent film for showing grasping acquisition region and alignment and semiclear film (white) for general experiments and demonstration. The Young's modulus of the film was tested approximately as 3.5 GPa following ASTM D882, and the Poisson's ratio was obtained from the manufacturer as 0.38. The thickness was measured as 0.127 mm. All the kirigami shells were digitally designed with Adobe Illustrator CS6 and then cut out from a flat PET sheet with a laser cutter (Epilog Legend Helix laser machine). Then, the sheet was mounted onto a steel bar with the desired radius and placed in oven at 80°C for 1 hour. The curvature was then measured with an image process technique. For the purpose of photographing the samples, red or orange colored adhesive film was added on top of some PET films. No measurement was taken from these colored films.

Tensile and holding tests

Force and displacement for both tensile and holding tests were measured using Instron 5940 single column testing platform (fig. S8). For tensile test, two acrylic plates (McMaster-Carr) were cut and glued (Loctite 403) to the two ends of the kirigami shell. Then, the sample was mounted onto the test platform. The same approach was used to fabricate holding test samples. The sample was then mounted onto a house-built linear stage with a 3D-printed object enveloped inside (fig. S8C). The sphere was connected to the Instron with a Nylon string. The string pulled the sphere at a rate of 0.1 mm/s. The displacement versus pulling force relations were recorded automatically by the software that comes with Instron. Because of the size limitation of our laser cutting machine and test apparatus, we selected four pairs of geometric parameters ($\ell_c/\ell_x = 2.5$, $\ell_c/\ell_y = 2.5$), ($\ell_c/\ell_x = 3.5$, $\ell_c/\ell_y = 2.0$), ($\ell_c/\ell_x = 5.0$, $\ell_c/\ell_y = 2.0$), and ($\ell_c/\ell_x = 5.0$, $\ell_c/\ell_y = 1.5$) across the ℓ_c/λ_g landscape to fabricate the shell grippers for testing. Here, the slit length was 15 mm for all samples. For each gripper sample, holding force measurements were repeated five times. The results were averaged.

Force transmission

Pinching-actuation force transmission was measured with the Instron 5940 and a flexible force sensor (Tekscan FlexiForce OEM), as shown in fig. S8B. At a given actuation force measured with load cell on the Instron, the pinching force was measured with a Tekscan force sensor. Data were manually recorded. The force transmission was measured by the slope of the linear regression, as shown in fig. S6. To demonstrate the correlation between actuation force and pinching force, we selected three pairs of geometric parameters as ($\ell_c/\ell_x = 3.5$, $\ell_c/\ell_y = 2.0$), ($\ell_c/\ell_x = 5.0$, $\ell_c/\ell_y = 2.0$), and ($\ell_c/\ell_x = 5.0$, $\ell_c/\ell_y = 1.5$). Here, the slit length is 12 mm for all samples. Each sample was tested for about 100 given actuation forces, and the corresponding pinching forces were recorded. Then, linear regression was used to find the slope representing the force transmission.

Magnetic soft gripper

A molding approach was used to fabricate the soft gripper. The main body of the gripper was fabricated with PVS (Zhermack Elite Double 8). The embedded cellulose paper was classical cleanroom wipes (Texwipe TechniCloth Nonwoven Dry Wipers Texwipe TX609). This wipe paper was made of 45% polyester and 55% cellulose and

Downloaded from https://www.science.org at The Hong Kong University of Science and Technology (Guangzhou) on May 26, 2026

has a unidirectional fiber network. The magnetic tip was composed of PDMS (Dow Corning Sylgard 184 elastomer kit) mixed with iron particles (McMaster-Carr) in a weight ratio of 1:3 (uncured PDMS to iron particle). Magnetic field was generated by a high-pull NdFeB cylindrical permanent magnet and measured using a Gaussmeter (PCE-MFM 3000). The mechanical response of the fabricated gripper under uniaxial tension is shown in fig. S9A. The tests were performed five times using the Instron 5940, and the results were averaged. As observed, actuation force and extension required to close the gripper were 0.386 N and 11.5 mm, respectively. These values were used to estimate the required magnetic flux density (B) of the applied magnetic field. Figure S9B shows the gripper closing process under magnetic actuation as we turn on the house-built electromagnet. Because the cylindrical curvature plays a role as an imperfection to bias the shell deformation, it is not necessary to precisely control the curvature here.

SUPPLEMENTARY MATERIALS

robotics.sciencemag.org/cgi/content/full/6/54/eabd6426/DC1
Note S1. Pattern selection of kirigami shell.
Note S2. Numerical simulations.
Note S3. Variation of appendages.
Note S4. Evaluation of friction.
Note S5. Theoretical modeling.
Note S6. Grasping acquisition region.
Fig. S1. Geometry and deformation of kirigami patterned sheet versus kirigami patterned shell.
Fig. S2. Effect of tab configuration on shape-morphing of kirigami shell.
Fig. S3. Simplification of mechanical modeling guided by finite element simulation.
Fig. S4. Demonstration of the variation of gripper appendages.
Fig. S5. Effect of friction on pulling force.
Fig. S6. Force transmission between actuation and pinching.
Fig. S7. Investigation of gripper grasping region.
Fig. S8. Images demonstrating experimental setup for measuring actuation force, pulling force, and pinching force.
Fig. S9. Magnetically actuated kirigami shell gripper.
Movie S1. Kirigami shells grasping various objects with distinct shape, size, and mechanical properties.
Movie S2. Finite element simulations showing shape morphing of kirigami shell.
Movie S3. Finite element simulations showing energy evolution of kirigami gripper as object is pulled out.
Movie S4. Gripper array transfers 24 hydrogel spheres simultaneously.
Movie S5. Magneto kirigami gripper capturing free-falling stone.

REFERENCES AND NOTES

1. T. Feix, J. Romero, H. Schmiedmayer, A. M. Dollar, D. Kragic, The GRASP taxonomy of human grasp types. *IEEE Trans. Hum. Mach. Syst.* **46**, 66–77 (2016).
2. A. Bicchi, V. Kumar, Robotic grasping and contact: A review, in *Proceedings 2000 ICRA. Millennium Conference. IEEE International Conference on Robotics and Automation. Symposia Proceedings* (*Cat. No.00CH37065*) (IEEE, 2000), vol. 1, pp. 348–353.
3. R. Hodson, How robots are grasping the art of gripping. *Nature* **557**, S23–S25 (2018).
4. M. Cianchetti, C. Laschi, A. Menciassi, P. Dario, Biomedical applications of soft robotics. *Nat. Rev. Mater.* **3**, 143–153 (2018).
5. A. Pettersson, S. Davis, J. Gray, T. Dodd, T. Ohlsson, Design of a magnetorheological robot gripper for handling of delicate food products with varying shapes. *J. Food Eng.* **98**, 332–338 (2010).
6. C.-Y. Chu, R. M. Patterson, Soft robotic devices for hand rehabilitation and assistance: A narrative review. *J. Neuroeng. Rehabil.* **15**, 9 (2018).
7. N. R. Sinatra, C. B. Teeple, D. M. Vogt, K. K. Parker, D. F. Gruber, R. J. Wood, Ultragentle manipulation of delicate structures using a soft robotic gripper. *Sci. Robot.* **4**, eaax5425 (2019).
8. J. Zhou, S. Chen, Z. Wang, A soft-robotic gripper with enhanced object adaptation and grasping reliability. *IEEE Robot. Autom. Lett.* **2**, 2287–2293 (2017).
9. Y. Hao, Z. Gong, Z. Xie, S. Guan, X. Yang, Z. Ren, T. Wang, L. Wen, Universal soft pneumatic robotic gripper with variable effective length, in *2016 35th Chinese Control Conference* (*CCC*) (IEEE, 2016), pp. 6109–6114.
10. T. Yoshimi, N. Iwata, M. Mizukawa, Y. Ando, Picking up operation of thin objects by robot arm with two-fingered parallel soft gripper, in *2012 IEEE Workshop on Advanced Robotics and Its Social Impacts* (*ARSO*) (IEEE, 2012), pp. 7–12.
11. Z. Xu, E. Todorov, Design of a highly biomimetic anthropomorphic robotic hand towards artificial limb regeneration, *2016 IEEE International Conference on Robotics and Automation* (*ICRA*) (IEEE, 2016), pp. 3485–3492.
12. R. Deimel, O. Brock, A novel type of compliant and underactuated robotic hand for dexterous grasping. *Int. J. Robot. Res.* **35**, 161–185 (2016).
13. E. Brown, N. Rodenberg, J. Amend, A. Mozeika, E. Steltz, M. R. Zakin, H. Lipson, H. M. Jaeger, Universal robotic gripper based on the jamming of granular material. *Proc. Natl. Acad. Sci.* **107**, 18809–18814 (2010).
14. C. B. Teeple, T. N. Koutros, M. A. Graule, R. J. Wood, Multi-segment soft robotic fingers enable robust precision grasping. *Int. J. Robot. Res.* **39**, 1647–1667 (2020).
15. T. Nishimura, K. Mizushima, Y. Suzuki, T. Tsuji, T. Watanabe, Variable-grasping-mode underactuated soft gripper with environmental contact-based operation. *IEEE Robot. Autom. Lett.* **2**, 1164–1171 (2017).
16. M. R. Cutkosky, On grasp choice, grasp models, and the design of hands for manufacturing tasks. *IEEE Trans. Robot. Autom.* **5**, 269–279 (1989).
17. H. K. Yap, H. Y. Ng, C.-H. Yeow, High-force soft printable pneumatics for soft robotic applications. *Soft Robot.* **3**, 144–158 (2016).
18. B. Mosadegh, P. Polygerinos, C. Keplinger, S. Wennstedt, R. F. Shepherd, U. Gupta, J. Shim, K. Bertoldi, C. J. Walsh, G. M. Whitesides, Pneumatic networks for soft robotics that actuate rapidly. *Adv. Funct. Mater.* **24**, 2163–2170 (2014).
19. F. Ilievski, A. D. Mazzeo, R. F. Shepherd, X. Chen, G. M. Whitesides, Soft robotics for chemists. *Angew. Chem. Int. Ed.* **50**, 1890–1895 (2011).
20. G. M. Whitesides, Soft robotics. *Angew. Chem. Int. Ed.* **57**, 4258–4273 (2018).
21. D. B. Camarillo, C. R. Carlson, J. K. Salisbury, Configuration tracking for continuum manipulators with coupled tendon drive. *IEEE Trans. Robot.* **25**, 798–808 (2009).
22. L. Hines, K. Petersen, G. Z. Lum, M. Sitti, Soft actuators for small-scale robotics. *Adv. Mater.* **29**, 1603483 (2017).
23. O. M. Wani, H. Zeng, A. Priimagi, A light-driven artificial flytrap. *Nat. Commun.* **8**, 15546 (2017).
24. A. Lendlein, O. E. C. Gould, Reprogrammable recovery and actuation behaviour of shape-memory polymers. *Nat. Rev. Mater.* **4**, 116–133 (2019).
25. S. Shian, K. Bertoldi, D. R. Clarke, Dielectric elastomer based "grippers" for soft robotics. *Adv. Mater.* **27**, 6814–6819 (2015).
26. A. Crivaro, R. Sheridan, M. Frecker, T. W. Simpson, P. V. Lockette, Bistable compliant mechanism using magneto active elastomer actuation. *J. Intell. Mater. Syst. Struct.* **27**, 2049–2061 (2016).
27. W. Johannisson, R. Harnden, D. Zenkert, G. Lindbergh, Shape-morphing carbon fiber composite using electrochemical actuation. *Proc. Natl. Acad. Sci. U.S.A.* **117**, 7658–7664 (2020).
28. D. P. Holmes, Elasticity and stability of shape-shifting structures. *Curr. Opin. Colloid Interface Sci.* **40**, 118–137 (2019).
29. J. Shintake, V. Cacucciolo, D. Floreano, H. Shea, Soft robotic grippers. *Adv. Mater.* **30**, 1707035 (2018).
30. J. Hughes, U. Culha, F. Giardina, F. Guenther, A. Rosendo, F. Iida, Soft manipulators and grippers: A review. *Front. Robot. AI* **3**, 69 (2016).
31. L. L. Howell, S. P. Magleby, B. M. Olsen, *Handbook of Compliant Mechanisms* (John Wiley & Sons Ltd., 2013).
32. L. L. Howell, *Compliant Mechanisms* (John Wiley & Sons Ltd., 2001).
33. D. Rus, M. T. Tolley, Design, fabrication and control of origami robots. *Nat. Rev. Mater.* **3**, 101–112 (2018).
34. S.-J. Kim, D.-Y. Lee, G.-P. Jung, K.-J. Cho, An origami-inspired, self-locking robotic arm that can be folded flat. *Sci. Robot.* **3**, eaar2915 (2018).
35. H. C. Greenberg, M. L. Gong, S. P. Magleby, L. L. Howell, Identifying links between origami and compliant mechanisms. *Mech. Sci.* **2**, 217–225 (2011).
36. S. Kota, K. J. Lu, Z. Kreiner, B. Trease, J. Arenas, J. Geiger, Design and application of compliant mechanisms for surgical tools. *J. Biomech. Eng.* **127**, 981–989 (2005).
37. M. Isobe, K. Okumura, Initial rigid response and softening transition of highly stretchable kirigami sheet materials. *Sci. Rep.* **6**, 24758 (2016).
38. A. Rafsanjani, K. Bertoldi, Buckling-induced kirigami. *Phys. Rev. Lett.* **118**, 084301 (2017).
39. G. P. T. Choi, L. H. Dudte, L. Mahadevan, Programming shape using kirigami tessellations. *Nat. Mater.* **18**, 999–1004 (2019).
40. P. D. Holmes, Y. Yang, A cut above: Folding and cutting advanced materials. *Matter* **1**, 799–800 (2019).
41. Y. Tang, Y. Li, Y. Hong, S. Yang, J. Yin, Programmable active kirigami metasheets with more freedom of actuation. *Proc. Natl. Acad. Sci. U.S.A.* **116**, 26407–26413 (2019).
42. A. Lamoureux, K. Lee, M. Shlian, S. R. Forrest, M. Shtein, Dynamic kirigami structures for integrated solar tracking. *Nat. Commun.* **6**, 8092 (2015).
43. T. C. Shyu, P. F. Damasceno, P. M. Dodd, A. Lamoureux, L. Xu, M. Shlian, M. Shtein, S. C. Glotzer, N. A. Kotov, A kirigami approach to engineering elasticity in nanocomposites through patterned defects. *Nat. Mater.* **14**, 785–789 (2015).
44. M. K. Blees, A. W. Barnard, P. A. Rose, S. P. Roberts, K. L. McGill, P. Y. Huang, A. R. Ruyack, J. W. Kevek, B. Kobrin, D. A. Muller, P. L. McEuen, Graphene kirigami. *Nature* **524**, 204–207 (2015).

Downloaded from https://www.science.org at The Hong Kong University of Science and Technology (Guangzhou) on May 26, 2026

45. L. Xu, T. C. Shyu, N. A. Kotov, Origami and kirigami nanocomposites. *ACS Nano* **11**, 7587–7599 (2017).
46. Y. Yang, M. A. Dias, D. P. Holmes, Multistable kirigami for tunable architected materials. *Phys. Rev. Mater.* **2**, 110601 (2018).
47. W. Wang, C. Li, H. Rodrigue, F. Yuan, M. W. Han, M. Cho, S. H. Ahn, Kirigami/origami-based soft deployable reflector for optical beam steering. *Adv. Funct. Mater.* **27**, 1604214 (2017).
48. Y. Morikawa, S. Yamagiwa, H. Sawahata, R. Numano, K. Koida, M. Ishida, T. Kawano, Ultrastretchable kirigami bioprobes. *Adv. Healthc. Mater.* **7**, 1701100 (2018).
49. Y.-S. Guan, Z. Zhang, Y. Tang, J. Yin, S. Ren, Kirigami-inspired nanoconfined polymer conducting nanosheets with 2000% stretchability. *Adv. Mater.* **30**, 1706390 (2018).
50. K. Yong, S. de, E. Y. Hsieh, J. Leem, N. R. Aluru, S. W. Nam, Kirigami-inspired strain-insensitive sensors based on atomically-thin materials. *Mater. Today* **34**, 58–65 (2020).
51. S. Song, M. Sitti, Soft grippers using micro-fibrillar adhesives for transfer printing. *Adv. Mater.* **26**, 4901–4906 (2014).
52. A. Carlson, A. M. Bowen, Y. Huang, R. G. Nuzzo, J. A. Rogers, Transfer printing techniques for materials assembly and micro/nanodevice fabrication. *Adv. Mater.* **24**, 5284–5318 (2012).
53. C. R. Calladine, *Theory of Shell Structures* (Cambridge Univ. Press, 2010).
54. X.-Y. Zhang, Y. Nakamura, K. Goda, K. Yoshimoto, Robustness of power grasp, in *Proceedings of the 1994 IEEE International Conference on Robotics and Automation* (IEEE, 1994), vol. 4, pp. 2828–2835.
55. D. M. Aukes, M. R. Cutkosky, Simulation-based tools for evaluating underactuated hand designs, in *2013 IEEE International Conference on Robotics and Automation* (IEEE, 2013), pp. 2067–2073.
56. S. I. Rich, R. J. Wood, C. Majidi, Untethered soft robotics. *Nat. Electronics* **1**, 102–112 (2018).
57. M. Sitti, H. Ceylan, W. Hu, J. Giltinan, M. Turan, S. Yim, E. Diller, Biomedical applications of untethered mobile milli/microrobots. *Proc. IEEE* **103**, 205–224 (2015).

Funding: We gratefully acknowledge the financial support from NSF through CMMI-1824882.
Author contributions: Y.Y. and D.P.H. conceived the concept. Y.Y. and K.V. conducted the experiments. Y.Y. performed data analysis, simulation, and modeling. Y.Y. and D.P.H. wrote the paper. **Competing interests:** Y.Y. and D.P.H. are inventors on a patent (US10933539) that covers the grasping methods and related devices. K.V. declares that they have no competing interests. **Data and materials availability:** All data needed to evaluate the conclusions in the paper are present in the paper or the Supplementary Materials.

Submitted 23 July 2020
Accepted 19 April 2021
Published 12 May 2021
10.1126/scirobotics.abd6426

Citation: Y. Yang, K. Vella, D. P. Holmes, Grasping with kirigami shells. *Sci. Robot.* **6**, eabd6426 (2021).

Downloaded from https://www.science.org at The Hong Kong University of Science and Technology (Guangzhou) on May 26, 2026

Science Robotics

Grasping with kirigami shells

Yi Yang, Katherine Vella, and Douglas P. Holmes

Sci. Robot. **6** (54), eabd6426. DOI: 10.1126/scirobotics.abd6426

View the article online
https://www.science.org/doi/10.1126/scirobotics.abd6426
Permissions
https://www.science.org/help/reprints-and-permissions

Downloaded from https://www.science.org at The Hong Kong University of Science and Technology (Guangzhou) on May 26, 2026

Use of this article is subject to the Terms of service

Science Robotics (ISSN 2470-9476) is published by the American Association for the Advancement of Science. 1200 New York Avenue NW, Washington, DC 20005. The title *Science Robotics* is a registered trademark of AAAS.

Copyright © 2021 The Authors, some rights reserved; exclusive licensee American Association for the Advancement of Science. No claim to original U.S. Government Works